

## THE EFFECT OF AGEING ON MICROSTRUCTURE AND MICROHARDNESS OF FULLY LAMELLAR Ti-45Al-5Nb-0.2B-0.75C ALLOY

ČEGAN Tomáš<sup>1,2</sup>, LAPIN Juraj<sup>2</sup>, SZURMAN Ivo<sup>1</sup>, NOSKO Martin<sup>2</sup>

<sup>1</sup>VŠB-Technical University of Ostrava, Faculty of Metallurgy and Materials Engineering,  
Department of RMSTC, 17. listopadu 15, 708 33 Ostrava – Poruba, Czech Republic, EU

<sup>2</sup>Institute of Materials and Machine Mechanics, Slovak Academy of Sciences, Račianska 75, 831 02  
Bratislava 3, Slovak Republic, EU, tomas.cegan@savba.sk

### Abstract

The effect of ageing on microstructure and Vickers microhardness of fully lamellar Ti-45Al-5Nb-0.2B-0.75C (at.%) alloy was studied. The experimental procedure for preparation of the studied alloy included induction melting of pure elements, centrifugal casting of cylindrical bars and hot isostatic pressing of the bars to eliminate porosity. A fully lamellar  $\gamma(\text{TiAl})/\alpha_2(\text{Ti}_3\text{Al})$  microstructure of the samples was achieved by the heat treatment consisting of solid solution annealing in a single  $\alpha$  phase field followed by the cooling to room temperature. The ageing experiments were performed at three different temperatures of 750, 850 and 950 °C up to 650 h in protective argon atmosphere. During the ageing the Vickers microhardness first increases with increasing ageing time and after reaching maximum values it decreases. The microstructure analysis by optical microscopy, scanning electron microscopy and X-ray diffraction analysis (XRD) show that the variations of measured microhardness values with the ageing time are connected with precipitation hardening. The peak microhardness values measured in the samples aged at 950 °C for 8 h are connected with the precipitation of carbides mainly of  $\text{Ti}_2\text{AlC}$  type. The age softening observed after the ageing at 950 °C for 650 h results from the coarsening of the carbides and partial dissolution of the  $\alpha_2$  lamellae.

**Keywords:** titanium aluminides, microstructure, carbides, precipitation hardening, microhardness

### 1. INTRODUCTION

The intermetallic alloys based on  $\gamma$ -TiAl have been intensively studied as high temperature materials because of their low density, high melting temperature, good corrosion resistance, creep strength and acceptable price/properties ratio [1, 2]. Depending on the alloy composition and processing parameters, various microstructures can be obtained in this group of alloys. Alloys with fully lamellar type of microstructure are characterised by a better high temperature strength when compared to that of the alloys with near  $\gamma$  or duplex type of microstructure [3]. However, their creep resistance at high temperatures (above 800 °C) does not fulfil requirements of designers which hinders their some perspective applications e.g. for turbocharger wheels of gasoline engines. Further possibility for increasing the creep resistance can be achieved by an optimisation of their chemical composition through solid solution and precipitation hardening. It is well established that substitutional elements like Nb, Ta, Mo as well as interstitial element C improve creep resistance of TiAl-based alloys. Alloying by Nb, Ta and Mo leads to reduced diffusivity and retarded thermal activated dislocation climb during creep [4-6]. Additions of C results in a precipitation hardening through formation of carbide particles of TiAl-based matrix. Coherent  $\text{Ti}_3\text{AlC}$  (P-type) particles are formed at temperatures up to about 750 °C and incoherent  $\text{Ti}_2\text{AlC}$  (H-type) carbides at higher temperatures [6-8]. The carbide precipitation is greatly influenced by the carbon content and its solubility limit in the alloy [6, 9]. The solubility limit of carbon varies with Al content and alloying elements [10].

The aim of this article is to study the effect of ageing on microstructure and Vickers microhardness of fully lamellar Ti-45Al-5Nb-0.2B-0.75C (at.%) alloy.

## 2. EXPERIMENT

The selected alloy was produced by vacuum induction melting in graphite crucible from pure metals (4N) and Nb-Al master alloy, which preparation, chemical composition and melting temperature were described elsewhere [11]. Table 1 shows nominal and measured chemical composition of the cast cylindrical sample with a diameter of 20 mm and length of 225 mm. A detailed description of the centrifugal casting and applied casting conditions were the same as described recently in [12]. The as-cast cylindrical bars were subjected to a hot isostatic pressing (HIP) at an applied pressure of 180 MPa and temperature of 1270 °C for 4 h in order to eliminate casting porosity. A fully lamellar  $\gamma(\text{TiAl})/\alpha_2(\text{Ti}_3\text{Al})$  microstructure of the bar was produced by heat treatment consisting of solution annealing and cooling to room temperature. The solid solution annealing was performed in a single  $\alpha$  phase (Ti-based solid solution with hexagonal crystal structure) field at 1360 °C for 1 h followed by cooling at a constant cooling rate of 20 °C/min to 850 °C under argon atmosphere. The heat treatment was accomplished by the cooling to room temperature in air. After the heat treatment, the bar was cut by electro spark machining into small pieces with a diameter of 20 mm and length of 12 mm. The ageing experiments were performed at three temperatures of 750, 850 and 950 °C up to 650 h in resistance tube furnaces with static argon atmosphere. For metallographic preparation of the samples, standard techniques such as grinding on SiC papers with grain sizes ranging from 80 to 2000 and polishing with diamond suspensions with particle size changing from 5 to 0.3  $\mu\text{m}$  were applied. The samples were observed by optical microscopy on the microscope Olympus GX51 equipped with digital camera Olympus DP12 (OM), scanning electron microscopy in the mode of back-scattered electrons (BSEM) using microscopes QUANTA FEG 450 and JSM-7600F equipped with an energy dispersive spectrometer (EDS) and by X-ray diffraction (XRD). Transmission electron microscopy (TEM) was performed by JEM-2100 microscope operating at 200 kV. Samples for TEM with an initial thickness of 0.3 mm were thinned mechanically by grinding to a thickness of 100  $\mu\text{m}$  and finally thinned electrolytically in electrolyte A3 Struers with using TenuPol-3 device operating at a voltage of 20 V and solution temperature of -20 °C. Oxygen and carbon contents were measured by thermo-evolution method by analysers ELTRA ONH-2000 and ELTRA CS-2000, respectively. Vickers microhardness measurements were performed at a constant load of 0.1 N for loading time of 10 s on polished and slightly etched samples. Quantitative metallographic analysis was performed on digitalized micrographs using a computerized image analyser SigmaScanPro. For the determination of porosity, the same procedure was used as described in [13].

**Tab. 1** Nominal and measured chemical composition of the alloy (at.%)

	Ti	Nb	Al	B	C	O
Nominal	Bal.	5	45	0.2	0.75	-
Measured	Bal.	5.21 ± 0.10	45.33 ± 1.13	-	0.69 ± 0.01	0.13 ± 0.02

## 3. RESULTS AND DISCUSSION

### 3.1 Microstructure of as-cast alloy

The measured chemical composition of the as-cast alloy is very close to the nominal composition, as seen in Table 1. The oxygen content of 0.13 at. % (490 wt. ppm) meets the requirements for the industrial applications where the maximum allowable oxygen content is usually reported to be about 500 wt. ppm [14]. Fig. 1 shows the typical microstructure of the as-cast alloy. The microstructure consists of columnar grains growing from the surface to the centre and some equiaxed grains in the middle of the bar. Fig. 2 shows the typical dendritic microstructure of the alloy. The microstructure is lamellar consisting of  $\gamma(\text{TiAl})/\alpha_2(\text{Ti}_3\text{Al})$  phases, as shown in Fig. 3. White colour network within the dendrites belongs to  $\beta$  phase (Ti-based solid solution with cubic crystal structure), which is enriched with Nb and depleted with Al (6.8 ± 1.1 at. % Nb, 37.6 ± 3.4 at. %Al). Small amount of  $\gamma$ -phase (dark colour phase) enriched with Al and depleted with Nb (4.35 ±

1.29 at. % Nb,  $50.43 \pm 3.88$  at. %Al) is formed in the inter-dendritic region. Particles with ribbon-like morphology are identified as (Ti,Nb)B borides, which is in agreement with the observations of similar type of alloys [15, 16]. Shrinkage porosity is formed inside the bar mainly in the interdendritic areas during solidification, as seen in Figs. 2 and 3. The highest volume fraction of pores (about 4 vol.%) and the large pores (until  $0.1 \text{ mm}^2$ ) are observed in the central part of the bar, as seen in Fig. 4.

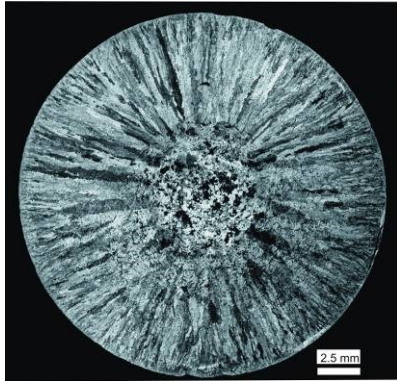


Fig. 1 Macrostructure of as-cast alloy.

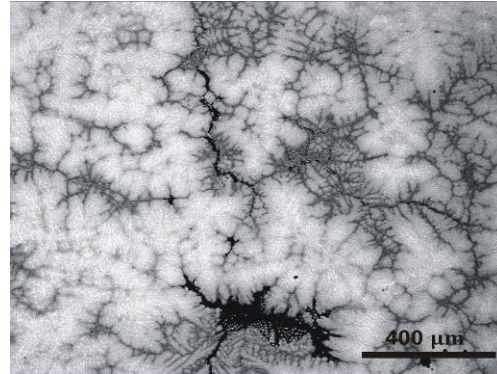


Fig. 2 Dendritic microstructure of as-cast alloy, BSEM.

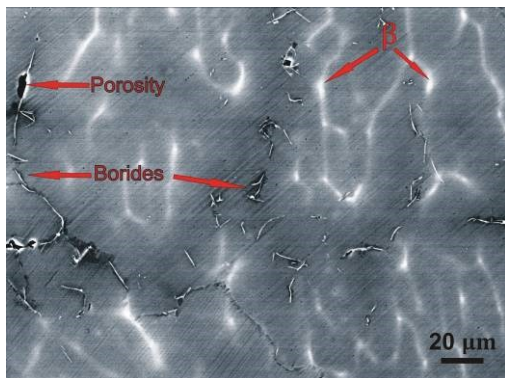


Fig. 3 Lamellar  $\gamma/\alpha_2$  microstructure with boride particles of as-cast alloy.

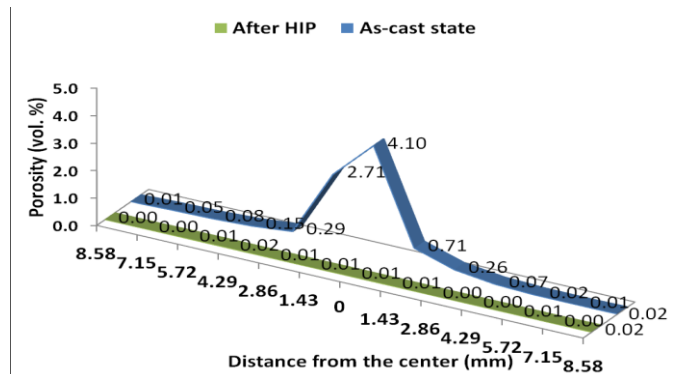


Fig. 4 Distribution of porosity on transversal section of as-cast cylindrical bar.

### 3.2 Microstructure of alloy after HIP

The porosity in any part of the HIP-ed cylindrical bar (including the central region) does not exceed values above 0.02 vol. % with maximum pore diameter of  $30 \mu\text{m}^2$ . Fig. 5 shows the microstructure after HIP. The microstructure consists mainly of lamellar  $\gamma/\alpha_2$  regions and some small equiaxed  $\gamma$  grains with the composition ( $4.91 \pm 0.07$ ) at.% Nb and ( $50.53 \pm 0.29$ ) at.% Al. The  $\beta$ -phase was completely dissolved during HIP at  $1270 \text{ }^\circ\text{C}$  corresponding to two phase  $\gamma + \alpha_2$  field of the studied alloy.

### 3.3 Microstructure of heat treated alloy

Fig. 6 shows the microstructure of the alloy after solid solution annealing followed by the cooling at a constant cooling rate of  $20 \text{ }^\circ\text{C}/\text{min}$  to  $850 \text{ }^\circ\text{C}$  and free air cooling to room temperature. The microstructure consists of equiaxed grains with an average size of  $385 \mu\text{m}$ . The microstructure of the grains is fully lamellar with average width of the  $\gamma$  and  $\alpha_2$  lamellae of ( $0.31 \pm 0.04$ ) and ( $0.42 \pm 0.04$ )  $\mu\text{m}$ , respectively. Quantitative metallographic analysis revealed that the lamellar grains contain about 37 vol.% of the  $\alpha_2$  phase and 63 vol.% of the  $\gamma$  phase. These results are in a good agreement with the results reported by Schwaighofer [6] for the TNM alloy with 0.75 at.% C. Relatively high volume fraction of the  $\alpha_2$  phase can be explained by a stabilizing effect of carbon [6, 9]. Fig. 7 shows TEM bright field image of alloy after the heat treatment. In this

figure, the lamellae contain no carbides, which clearly indicates that carbon remained completely dissolved in the  $\gamma$  and  $\alpha_2$  phases after the applied heat treatment.

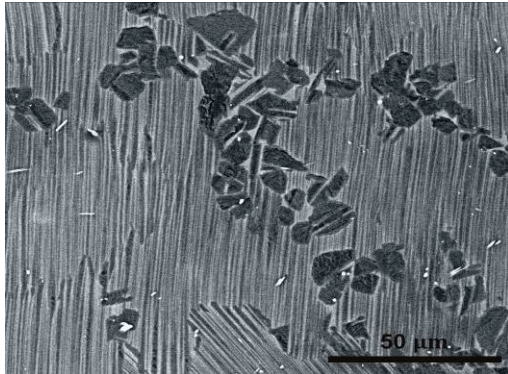


**Fig. 5** Microstructure after HIP (BSEM).



**Fig. 6** Microstructure after heat treatment (OM).

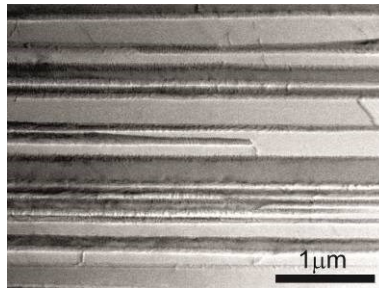
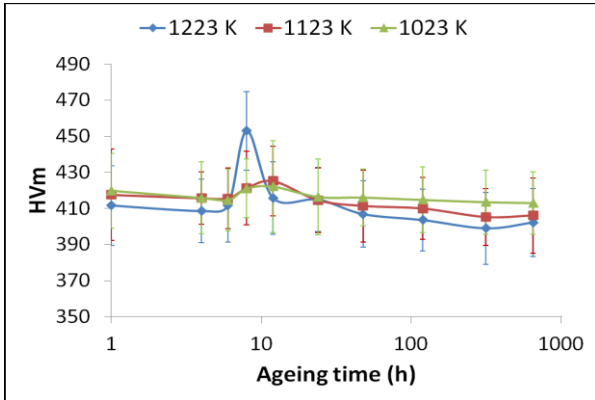


**Fig. 7** Bright field image of microstructure after heat treatment (TEM).

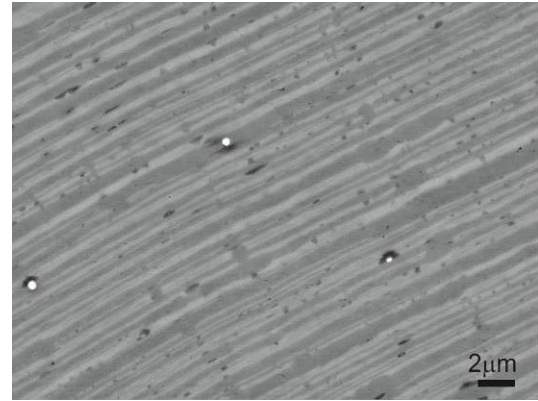
### 3.4 Microstructure and Vickers microhardness after ageing

Fig. 8 shows the variation of Vickers microhardness with the ageing time. The typical age hardening and softening are observed for all three ageing temperatures. During the age hardening the microhardness increases with the ageing time reaching maximum values at 8 h after ageing at 950 °C. The peak microhardness values for the samples aged at 750 and 850 °C are situated somewhere between 10 and 24 h and further experiments are still required to determine precisely the peak ageing time. Fig. 9 shows the microstructure after ageing at 950 °C for 8 h. A uniform distribution of fine precipitates can be observed in the lamellar  $\gamma/\alpha_2$  matrix. These precipitates are mainly formed at the lamellar interfaces and inside the  $\alpha_2$  lamellae. The XRD analysis (Fig. 10) shows occurrence of  $Ti_2AlC$  and  $Ti_3AlC$  carbides in the microstructure. The presence of the carbides is confirmed also the EDS analysis, which reveals an increased content of C in precipitates. An average size and volume fraction of the carbides is measured to  $(110 \pm 10)$  nm and 2.3 vol. %, respectively. Fig. 11 shows the microstructure after ageing at 950 °C for 650 h. The microstructure contains 2.2 vol. % of coarser carbides with an average size of  $(520 \pm 15)$  nm distributed mainly within the  $\alpha_2$  lamellae. The image analysis revealed that the ageing at 950 °C for 650 h leads to the partial dissolution of the  $\alpha_2$  lamellae and decrease of their volume fraction from 37 to 21 vol.% and thickness from  $(0.31 \pm 0.04)$  to  $(0.23 \pm 0.03)$   $\mu$ m. The formation of the carbides at 950 °C can be explained by the dissolution of  $\alpha_2$  lamellae. The  $\alpha_2$  phase has a significantly higher solubility of carbon than the  $\gamma$  phase which leads to the precipitation of the carbides at the  $\gamma/\alpha_2$  interfaces to achieve thermodynamic equilibrium state of the alloy at the ageing temperature. SEM observations show only very small amount of carbides after ageing at 850 °C and practically no carbides at 750 °C (Fig. 12). However, the increase of the microhardness values at 750 and 850 °C indicates the hardening. The age hardening at these temperatures results probably from the

precipitation of very fine p-type of carbides, which are under the resolution of SEM and might be identified using TEM techniques as the next step of this work.



**Fig. 8** Variation of Vickers microhardness  $HV_m$  with the ageing time.



**Fig. 9** Microstructure after ageing at 950 °C for 8 h (BSEM).

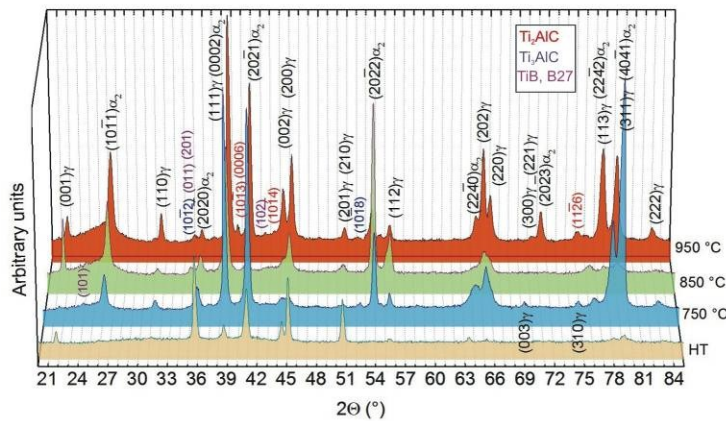


**Fig. 10** XRD patterns after heat treatment and ageing at 750, 850 and 950 °C for 8 h.

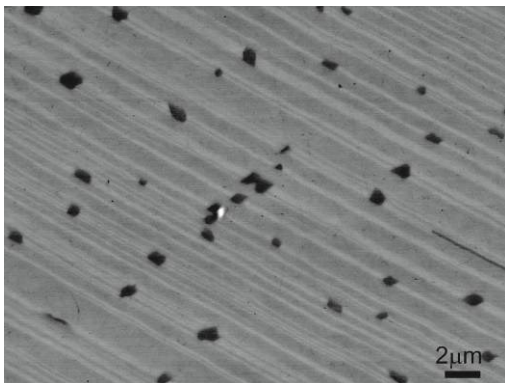


**Fig. 11** Microstructure after ageing at 950 °C for 650 h (BSEM).



**Fig. 12** Microstructure after ageing at 750 °C for 650 h (BSEM).

#### 4. CONCLUSIONS

The effect of ageing on microstructure and Vickers microhardness of fully lamellar Ti-45Al-5Nb-0.2B-0.75C (at.%) alloy was studied. During the ageing of Ti-45Al-5Nb-0.2B-0.75C (at.%) alloy with fully lamellar  $\gamma(\text{TiAl})/\alpha_2(\text{Ti}_3\text{Al})$  microstructure the Vickers microhardness first increases with increasing ageing time and

after reaching maximum values it decreases at all studied temperatures. TEM, SEM and XRD analysis revealed that the variations of the measured microhardness values with the ageing time are connected with microstructural instabilities. The peak microhardness values measured in the samples aged at 950 °C for 8 h are connected with the precipitation of carbides mainly of Ti<sub>2</sub>AlC type preferentially at the  $\gamma/\alpha_2$  interfaces. The age softening observed after the ageing at 950 °C for 650 h results from the coarsening of the carbides and partial dissolution of the  $\alpha_2$  lamellae. The formation of carbides at 950 °C can be explained by the dissolution of the  $\alpha_2$  phase with a significantly higher solubility of carbon than the  $\gamma$  phase and achieving thermodynamic equilibrium state of the heat treated alloy at the ageing temperature.

## ACKNOWLEDGEMENTS

**This article has been elaborated in the framework of the project Center for Applied Research of New Materials and Technology Transfer, ITMS 26240220088, supported by the Science and Research Operational Program by the European Regional Development Funds.**

## REFERENCES

- [1] LORIA, E.A. Quo vadis gamma titanium aluminide. *Intermetallics*, Vol. 8, No. 9-11, 2000, pp. 1339-1345.
- [2] TETSUI, T. Gamma Ti aluminides for non-aerospace application. *Curr. Opin. Solid State Mat. Sci.*, Vol. 4, No. 3, 1999, pp. 243-248.
- [3] APPEL, F. Microstructure and deformation of two-phase  $\gamma$ -titanium aluminides. *Materials Science and Engineering: R.*, Vol. 22, No. 5, 1998, pp. 187-268.
- [4] APPEL, F. Novel design concepts for gamma-base titanium aluminide alloys. *Intermetallics*, Vol. 8, No. 9-11, 2000, pp. 1283-1312.
- [5] LAPIN, J. TiAl-based alloys: Present status and future perspectives. In: *Metal 2009: 18th International Conference on Metallurgy and Materials*. Ostrava: TANGER, 2009, pp. 1-12.
- [6] SCHWAIGHOFER, E. Effect of carbon addition on solidification behavior, phase evolution and creep properties of an intermetallic  $\beta$ -stabilized  $\gamma$ -TiAl based alloy. *Intermetallics*, 46, Vol. 46, pp. 173-184.
- [7] KARADGE, M. Precipitation strengthening in K5-series  $\gamma$ -TiAl alloyed with silicon and carbon. *Metallurgical and material transactions A*, Vol. 34A, pp. 2129-2138.
- [8] TIAN, W.H. Effect of carbon addition on the microstructures and mechanical properties of  $\gamma$ -TiAl alloys. *Intermetallics*, Vol. 5, pp. 237-244.
- [9] PERDRIX, F. Relationships between interstitial content, microstructure and mechanical properties in fully lamellar Ti-48Al alloys, with special reference to carbon. *Intermetallics*, Vol. 9, 2001, pp. 807-815.
- [10] SCHEU, C. High carbon solubility in a  $\gamma$ -TiAl-based Ti-45Al-5Nb-0.5C alloy and its effect on hardening. *Acta Materialia*, Vol. 57, No. 5, 2009, pp. 1504-1511.
- [11] JUŘICA, J. Preparation and properties of master alloys Nb-Al and Ta-Al for melting and casting of gamma-TiAl intermetallics. *Materiali in Tehnologije/Materials and Technology*, 2015, Vol 49, No. 1, pp. 27-30.
- [12] ČEGAN, T. Preparation of TiAl-based alloys by induction melting in graphite crucibles. *Kovove mater.*, 2015, vol. 53, no. 2, pp. 69-78.
- [13] POHLUDKA, M. Porosity of Ni<sub>3</sub>Al based alloys prepared by gravity and centrifugal casting. In: *Metal 2012: 21th International Conference on Metallurgy and Materials*. Ostrava: TANGER, 2012, pp. 1547-1553.
- [14] ZOLLINGER, J. Influence of oxygen on solidification behaviour of cast TiAl-based alloys. *Intermetallics*, Vol. 15, No. 10, 2007, pp. 1343-1350.
- [15] KLIMOVA, A. Effect of solidification parameters on microsegregation behaviour of main alloying elements in a peritectic TiAl based alloy. *Kovove mater*, Vol. 51, No. 2, 2013, pp. 89-99.
- [16] HECHT, U. Grain refinement by low boron additions in niobium-rich TiAl-based alloys. *Intermetallics*, Vol. 16, No. 8, 2008, pp. 969-978.